SEGUE: A Speedy rEgion-Growing Algorithm for Unwrapping Estimated Phase

Anita Karsa[ID] and Karin Shmueli

Abstract—**Recent magnetic resonance imaging (MRI) techniques, such as quantitative magnetic susceptibility mapping, employ the signal phase to reveal disease-related changes in tissue composition, including iron or calcium content. The MRI phase is also routinely used in functional and diffusion MRI for distortion correction. However, phase images are wrapped into a range of 2π radians. Phase region expanding labeller for unwrapping discrete estimates (PRELUDE) is the gold standard method for robust, spatial, 3-D, MRI phase unwrapping. Unfortunately, PRELUDE's computation time can reach 15 min for a severely wrapped brain image and nearly 10 h to unwrap a full head-and-neck image on a standard PC. In this paper, we develop a Speedy rEgion-Growing algorithm for Unwrapping Estimated phase (SEGUE) based on similar principles to PRELUDE, implemented with additional methods for acceleration. We compared PRELUDE and SEGUE in numerical phantoms, and using *in vivo* images of the brain, head and neck, and pelvis acquired in 4–5 healthy volunteers and at 4–6 echo times. To overcome chemical-shift-induced errors within the head and neck, and pelvic images, we also investigated applying both techniques within fat and water masks separately. SEGUE provided almost identical unwrapped phase maps to the gold standard PRELUDE. SEGUE was (1.5 to 70 times) faster than PRELUDE, especially in severely wrapped images at later echoes and in the head and neck, and pelvic images. Applying these techniques within fat and water masks separately removed chemical-shift-induced errors successfully. SEGUE's MATLAB implementation is available for download. SEGUE is a general unwrapping algorithm not specific to MRI, and therefore could be used in images acquired with other modalities.**

Index Terms—**Diffusion, distortion correction, fMRI, functional, magnetic resonance imaging, MRI, phase unwrapping, QSM, susceptibility mapping.**

I. INTRODUCTION

THE phase component of the complex Magnetic Resonance Imaging (MRI) signal acquired with a

T_2^*-weighted gradient-echo sequence is proportional to the magnetic field inhomogeneities [1]. A range of techniques have recently been developed that exploit this property of the MRI phase including Susceptibility Weighted Imaging, a widely used clinical tool for visualizing veins, hemorrhages, and microbleeds [2], [3]. Furthermore, the recent increase in the use of high-field MRI systems has reinvigorated interest in phase imaging including the increasingly important field of Quantitative magnetic Susceptibility Mapping (QSM) [1], [4]–[7], a technique that can reveal disease-related changes in tissue iron, myelin and calcium content, and venous oxygenation [8]. Moreover, phase images are routinely used for distortion correction in functional MRI [9]–[13], diffusion MRI [14]–[17], and recently in MRI-based radiation therapy planning [18].

As the phase in MRI is defined as the angle of the magnetization vector in the complex (or transverse) plane, the measured MRI phase can only take values between 0 and 2π, introducing wraps (or 2π phase discontinuities) into the measured phase images (Fig. 1 a). At longer echo times, these phase images contain more spatial wraps (Figs. 5, 6, and 7 a).

Many algorithms have been developed to overcome this problem [19] but, among the robust, three-dimensional (3D), spatial phase unwrapping methods that provide a map of the total magnetic field inhomogeneities needed for distortion correction, Phase Region Expanding Labeller for Unwrapping Discrete Estimates (PRELUDE, [20]) in the FMRIB Software Library (FSL, [21]) is considered to be a gold standard as it is one of the most accurate [19] and widely used techniques. PRELUDE has been repeatedly shown to be able to unwrap standard brain images in a reasonable amount of time. However, depending on the image resolution, and field of view, at later echoes, the computation time (T_c) of PRELUDE can reach 15 minutes to unwrap a whole brain image (of 1 mm isotropic resolution, a field-of-view of 24 cm × 24 cm × 14.4 cm, acquired at echo time 24.6 ms) on a 64-bit Ubuntu Virtual Machine with a 3.5 GHz Processor and 16 GB RAM. Therefore, large-scale studies requiring distortion correction in the brain (e.g. for functional or diffusion MRI) would greatly benefit from accelerated phase unwrapping.

PRELUDE has been developed and optimized primarily for brain images, but recently, QSM has been increasingly applied in parts of the body other than the brain, e.g to detect calcifications in breast images, or measure liver iron content [22]–[26]. It can take up to 17 minutes for PRELUDE to unwrap a pelvic image and nearly 10 hours for a head-and-neck image using a standard PC with the aforementioned specifications.

Faster phase unwrapping would accelerate state-of-the-art research investigating a wide range of QSM applications. Moreover, these anatomical regions contain fatty areas as well as water-based tissue. The fatty areas have an additional, chemical-shift-induced phase component [22]. This can lead to errors in PRELUDE phase unwrapping that are yet to be addressed.

Here we develop a Speedy rEgion-Growing algorithm for Unwrapping Estimated phase (SEGUE) based on similar principles to PRELUDE, but with 1.5 to 70 times shorter T_c depending on the echo time and anatomical region. We also propose and investigate a simple, effective strategy for overcoming the chemical-shift-induced errors in the results of both PRELUDE and SEGUE. A MATLAB (Mathworks, Natick, MA, USA) implementation of SEGUE is downloadable from https://xip.uclb.com/i/software/SEGUE.html.

II. THEORY

A. PRELUDE

The PRELUDE algorithm [20] consists of two main steps: 1) partitioning and 2) unwrapping and merging. First, the phase map is partitioned into connected regions by dividing the $[0, 2\pi)$ interval into 6 smaller equal intervals (see e.g. Fig. 1 a and b). It is assumed that these regions do not contain any phase wraps. The wraps between these regions are unwrapped by adding an integer multiple of 2π to one of two neighboring regions assuming spatial smoothness of the phase and these neighboring regions are then merged. This process starts with the pair of neighboring regions in which the wrong phase offset would introduce the most error in the unwrapped phase image (e.g. a pair of regions with a large number of interfacing voxels on the border), and it continues until all the regions have been unwrapped and merged. The computation time is expected to be proportional to the number of initial regions.

In high resolution images, an initial region can erroneously contain a wrap if it consists of areas with a phase difference more than 2π connected by a few noisy voxels (see Fig. 1 a and b, red arrows). Moreover, the process of creating initial regions (see Fig. 9 a, dashed line) may result in an apparent wrap between two points within a region (see Fig. 9 a, A and B). A large, 3D initial region containing a wrap can have global, unpredictable effects on the resulting unwrapped phase map. To avoid this, PRELUDE limits the initial regions to be two dimensional (2D) for high-resolution images with a voxel size of 1 mm × 1 mm × 1 mm or smaller. However, slicing all the large, connected, 3D regions into smaller, 2D regions results in a greatly increased number of initial regions (that scales linearly with the number of slices in the 3D volume) and, consequently, very long computation time.

B. SEGUE

SEGUE provides an alternative way of unwrapping high-resolution phase images more rapidly than PRELUDE [27]. The process is accelerated by: 1) always using 3D regions to reduce the number of initial regions,
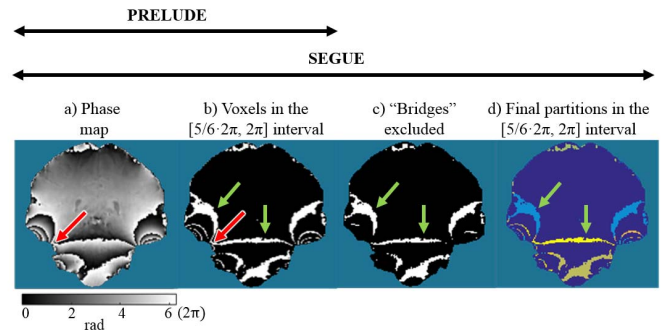

Fig. 1. Partitioning. PRELUDE: First, voxels with phase values (a) within one of the smaller phase intervals are identified (b). Then, the connected 2D regions are identified in each slice (not shown). 2D regions are used to avoid a phase difference more than 2π in the inital regions due to noisy voxels (red arrows with white border). SEGUE: The first step is the same as in PRELUDE (b). Then, instead of restricting the regions to 2D, the small bridges (red arrows with white border) connecting larger regions (green arrows) are excluded (c). Finally, the connected 3D regions (colours) are identified and the excluded voxels are assigned to the closest region in 3D (d).

2) unwrapping and merging multiple regions at the same time.

1) Partitioning: Similarly to PRELUDE, the $[0, 2\pi)$ interval is first divided into 6 smaller intervals (Fig. 1 b). Combined with the following scheme, we found that using 6 intervals provided the fewest wrap-free initial regions. At this stage, areas having a phase difference more than 2π (Fig. 1 b, green arrows) might be connected by a few noisy voxels (Fig. 1 a and b, red arrows). To avoid having initial regions containing a phase difference more than 2π, instead of restricting the regions to 2D as in PRELUDE, these small bridges between larger regions (Fig. 1 b, red arrow) are excluded before the connected 3D regions are determined (Fig. 1 c, green arrows). The excluded voxels are: i) located at the edges of the mask in Fig. 1 b, and ii) have zero-valued first, second, or third neighbors in at least two of the three (x, y, and z) directions. Finally, the connected, 3D regions are identified, assigned an integer identifier, and the excluded voxels are assigned to the initial regions that are closest to them in 3D (Fig. 1 d). Note that excluded voxels with two or more regions equally close are assigned to the one with the largest identifier. Also, smaller groups of voxels that are not connected to any of the regions are assigned their own integer identifier.

2) Unwrapping and Merging: Instead of comparing each adjacent pair of regions as in PRELUDE, the merging process in SEGUE starts by selecting the region with the largest border (Fig. 2, main region) and then gradually enlarging it by unwrapping all neighboring regions at the same time and merging these with the main region.

Phase values in the adjacent voxels (Fig. 2, highlighted in yellow) in neighboring regions, are estimated using linear extrapolation from two adjacent voxels (Fig. 2, red arrow), instead of nearest neighbor approximation as in PRELUDE. In theory, extrapolation should provide more accurate unwrapped phase maps near high susceptibility gradients. The extrapolated and measured phase values in these voxels are denoted by φ and Φ respectively. Phase values in the adjacent
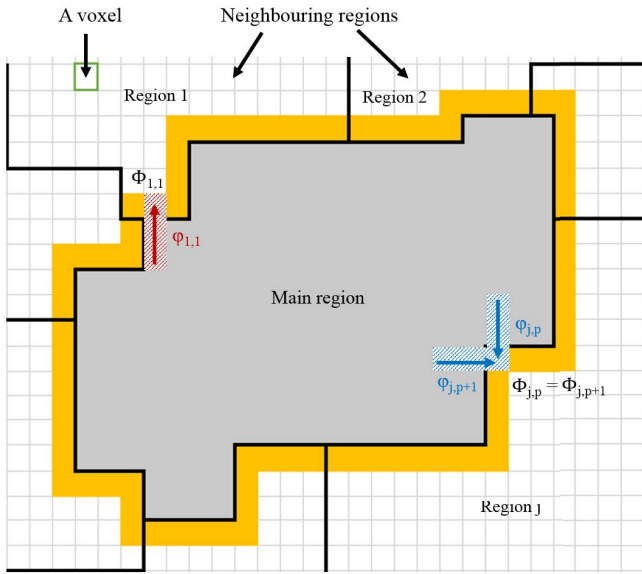
Fig. 2. Unwrapping and merging in SEGUE. Phase values in the voxels adjacent to the main region (yellow) are estimated using linear extrapolation (red arrow) from every possible direction (blue arrows). The phase offset is calculated from the differences between the extrapolated (φ) and the measured (Φ) phase values in the adjacent voxels.

voxels are extrapolated from every possible direction in 3D (Fig. 2, blue arrows).

The necessary phase offset for region j is calculated for each pair (p) of extrapolated and measured phase values by:

$$\Delta\varphi_{j,p} = 2\pi \cdot round\left(\frac{\varphi_{j,p} - \Phi_{j,p}}{2\pi}\right) \qquad (1)$$

The final phase offset for a given neighboring region j, $\Delta\varphi_j$, is determined by majority voting among all $\Delta\varphi_{j,p}$ values. This phase offset ($\Delta\varphi_j$) is applied to region j only if a substantial proportion ($P_{agree,j}$ from Eq. 2) of $\Delta\varphi_{j,p}$ values agree on the final phase offset and the unwrapped neighbouring regions are then merged with the main region. Eq. 2 describes a balance between the proportion of agreeing extrapolated and measured pairs ($P_{agree,j}$) and the amount of information we have about the neighbouring region j ($P_{border,j}$).

$$(1 - P_{limit}) \cdot P_{agree,j} \geq 1 - P_{border,j} \qquad (2)$$

$P_{agree,j}$ is the ratio of the number of p extrapolated and measured pairs where $\Delta\varphi_{j,p} = \Delta\varphi_j$ to the total number of all $\Delta\varphi_{j,p}$ values for a given neighbouring region j. $P_{border,j}$ is the ratio of the number of voxels on the border between region j and the main region, and the total number of voxels on the border of region j. P_{limit} is a preset value between 0 and 1. At one extreme, if all pairs agree (i.e. $P_{agree,j} = 100\%$), we need a substantial proportion of the border of region j to be shared with the main region (i.e. $P_{border,j} \geq P_{limit}$) to accept the phase shift. Therefore, if the regions are only connected by a few interfacing voxel pairs, unwrapping and merging is not performed even if all $\Delta\varphi_{j,p}$ values are the same. At the other extreme, if the main region completely surrounds region j (i.e. $P_{border,j} = 100\%$), we already have all the obtainable information about the border of region j,

so unwrapping and merging is performed regardless of the value of $P_{agree,j}$. $P_{limit} = 30\%$ was found to yield good results for most cases.

This process is repeated using the same enlarged main region until no more regions can be unwrapped and merged with it. Then, this main region is excluded from the unwrapping and the region with the second largest border is chosen as the next main region and the unwrapping and merging process continues. When at least a user-defined percentage (P_{req}) of the total volume in the tissue mask has been merged with one of the previous main regions, all of these are included in the unwrapping again and the merging process is repeated two more times with P_{limit} set to first 10% and then 0%. In the first cycle ($P_{limit} = 30\%$), even if all $\Delta\varphi_{j,p}$ values agree on the phase shift, $P_{border,j}$ needs to be larger than 30% (see Equation 2) for the region to be unwrapped and merged with the main region. While this enables the robust unwrapping of most regions, which is essential at the beginning of the algorithm, reducing P_{limit} is necessary to unwrap regions which do not share a large border with the main region due to the complicated anatomy. A three-cycle approach with $P_{limit} = 30\%$, 10%, and 0% was established by maximizing the number of unwrapped voxels in the acquired head-and-neck images. Note that in most brain images, more than 99% of the volume is merged with the first main region during the first cycle ($P_{limit} = 30\%$) of the algorithm.

The default value of P_{req} is 70%, but it can be set by the user. In general, a higher P_{req} provides more accurate phase maps, while a lower P_{req} results in faster unwrapping.

III. METHODS

SEGUE was developed in MATLAB R2015a, but it runs in all versions released between 2013 and 2017. Parallel computation has not been employed in this version but it might be possible to implement it in future versions to further accelerate the partitioning step. To test SEGUE, we compared its performance with PRELUDE in terms of unwrapping and computation time (T_c) by applying both techniques to simulated phase data and in-vivo MRI phase images of healthy volunteers.

A. Numerical Phantoms

First, we tested SEGUE's ability to resolve complicated phase patterns in a digital phantom with no noise as described by Robinson et al. [28] (complexity level = 4 and echo time = 10 ms).

To assess SEGUE's accuracy in noisy phase images, we used a 3D Gaussian distribution with varying noise levels as described in [19]. A 3D Gaussian (G) was embedded in a $256 \times 256 \times 256$ matrix with an amplitude of 1, and a full width at half maximum (FWHM) of 128 in each direction. This phase pattern was scaled using the following expression:

$$\phi = \gamma B_0 TE \cdot G \qquad (3)$$

where γ is the proton gyromagnetic ratio, $B_0 = 7$ T is the magnetic field, and TE = 16 ms is the echo time.

Gaussian-distributed noise was added to the real and imaginary components of $\exp(i\phi)$ (i.e. the simulated complex MRI signal). Noise amplitudes of 0.1, 0.2, 0.3, and 0.4 were used. This gave similar phase maps to those in [19].

B. Volunteer Images

To test SEGUE in a range of commonly scanned regions of the body, it was applied to phase images acquired in the brain, head-and-neck, or pelvis of healthy volunteers. While phase unwrapping is most commonly used in brain images, there has been increasing interest in phase imaging (e.g. QSM) in parts of the body outside of the brain. The acquired head-and-neck and pelvic images allowed us to test SEGUE in two different, but equally challenging anatomical regions and also investigate the performance of both SEGUE and PRELUDE in and around fatty tissue.

The local ethics committee approved this study and informed consent was obtained from all participants.

Multi-echo brain images were acquired in 5 healthy volunteers at 3 Tesla (Philips, Achieva, Netherlands), using a 32-channel head coil, a 3D, T_2^*-weighted gradient-echo sequence with monopolar readout gradients, matrix size = 240 × 240 × 144, Sensitivity Encoding (SENSE) acceleration factors = 1 × 2 × 1.5, 1 mm isotropic resolution, TE_1 = 3.0 ms, ΔTE = 5.4 ms, 5 echoes, repetition time = 29 ms, and flip angle = 20°.

Multi-echo head-and-neck images in another 4 healthy volunteers were also acquired using the same MRI system, a 16-channel head-and-neck coil and 3D gradient-echo sequence with monopolar readout gradients, matrix size = 220 × 220 × 240, SENSE factors = 1.5 × 2 × 1, 1 mm isotropic resolution, TE_1 = 3.0 ms, ΔTE = 5.3 ms, 4 echoes, repetition time = 23 ms, and flip angle = 18°.

Multi-echo images of the sacroiliac joint (pelvic images) acquired in 5 more healthy volunteers by Bray *et al.* [29] were also used to compare the two techniques. Multi-echo gradient-echo MRI with monopolar readout gradients was performed on a different 3-Tesla clinical system (Philips, Ingenia, Netherlands) using matrix size = 320 × 320 × 40, resolution = 1.56 × 1.56 × 2 mm, TE_1 = 1.17 ms, ΔTE = 1.6 ms, 6 echoes, repetition time = 25 ms, and flip angle = 3°.

C. Comparing PRELUDE and SEGUE

Both PRELUDE and SEGUE need tissue masks to identify the part of the image within which unwrapping needs to be performed. In the case of the complex phase topography, the entire 3D volume was unwrapped, while for the Gaussian phantoms, a sphere with a radius of 85 voxels was used. For the brain images, a mask was obtained using the FSL Brain Extraction Tool [30] on the last echo magnitude image. Masks for the head-and-neck and pelvic images were generated using a fixed threshold on the inverse noise maps calculated from the magnitude images across all the echoes [31].

All phase images were unwrapped using both PRELUDE and SEGUE and the results were evaluated using several

a) Ground truth	b) Wrapped phase	c) Unwrapped phase (SEGUE)	d) Difference (c - a)

1 h 41 m 58 s

-30 -15   0
rad

0   2   4   6
rad

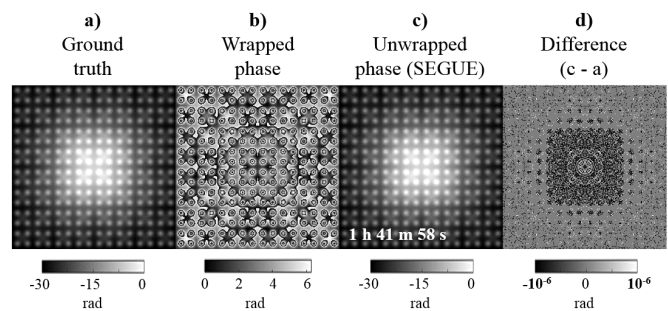-30   -15   0
rad

-10^{-6} 0 10^{-6}
rad

Fig. 3. Unwrapping a phase phantom with complex topography. Both PRELUDE and SEGUE were applied to the complex topography phase map (b). While PRELUDE failed to terminate within 3 days, SEGUE was able to provide an unwrapped phase image (c) in less than 102 minutes (T_c is shown in the corner of the unwrapped image). The difference map (d) between the SEGUE result (c) and the ground truth phase map (a) shows discrepancies only on a very small scale due to numerical precision errors. Slice 125 is shown in each case.

metrics: 1. Computation time (T_c) on a 64-bit Ubuntu Virtual Machine with a 3.5 GHz Processor and 16 GB RAM, 2. Percentage of unwrapped voxels within the tissue mask (UnVox), 3. Mean absolute error (ME) between the results and the ground truth for the numerical phantoms, and mean absolute difference (MD) between the PRELUDE and SEGUE results for the in-vivo images, 4. Percentage of voxels with different unwrapped phase (DiffVox) between the PRELUDE and SEGUE results (in the volunteer images only), 5. Maximum phase difference (MaxDiff) between the PRELUDE and SEGUE results (in the volunteer images only), and 6. Visual comparison of the unwrapped phase images.

D. Removing Chemical-Shift-Induced Phase Errors

In the head-and-neck and pelvic images, there is an additional, chemical-shift-induced phase difference between fatty and water-based voxels that could induce errors in both the PRELUDE and SEGUE unwrapped phase images. Here we tested a simple strategy for removing these errors; we tried applying both techniques separately in the fat and water masks to prevent the chemical-shift-induced fat-water phase difference from affecting the unwrapping process. In the head-and-neck images, fat-water separation was performed using the 3-point Dixon method [32] from the ISMRM fat-water separation toolbox [33]. In the pelvis, fat and water magnitude images had already been created by the vendor-supplied software (Philips mDixon Quant; Philips Healthcare, Andover, Massachusetts, USA). Each voxel within the original tissue mask was assigned to either the water or the fat mask depending on whether the water or the fat magnitude was larger in that particular voxel.

IV. RESULTS

The phase phantom of complex topography is shown in Fig. 3 a and b. It was successfully unwrapped using SEGUE (Fig. 3 c) in 101 minutes and 58 seconds while PRELUDE failed to terminate within 3 days and provided no results. The mean absolute error (ME) of the SEGUE result was 0.0002 rad

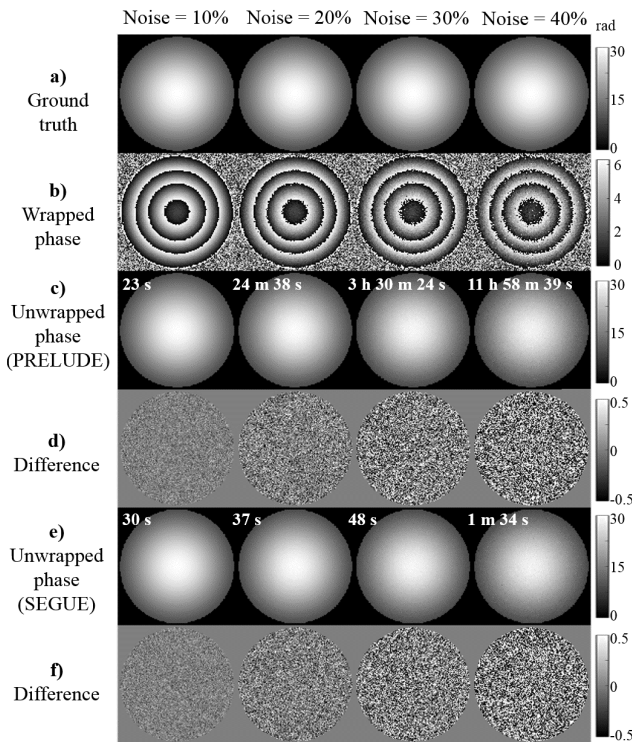|		PRELUDE			SEGUE		
	Noise level (%)	UnVox (%)	ME (rad)	T_c	UnVox (%)	ME (rad)	T_c
Complex	0	NA	NA	NA	100	0.0002	1 h 41 m 58 s
Gaussian	10	100	0.08	23 s	100	0.08	30 s
	20	100	0.16	24 m 38 s	100	0.16	37 s
	30	100	0.25	3 h 30 m 24 s	100	0.25	48 s
	40	100	0.34	11 h 58 m 39 s	100	0.34	1 m 34 s

Fig. 4. Unwrapping a Gaussian phantom. Phase maps of a Gaussian phantom with four different noise levels (a, b) were unwrapped using either PRELUDE (c) or SEGUE (e). T_c corresponding to each result is shown in the corner of the unwrapped phase maps. Difference images between the PRELUDE/SEGUE results and the ground truth phase maps (a) are also displayed (d and f respectively). All scales are in radians.

Table I shows that both techniques could unwrap 100% of the voxels in all numerical phantoms (except PRELUDE did not provide any results in the phantom of complex topography).

Figs. 5, 6, and 7 show the results of PRELUDE and SEGUE in the brain, head-and-neck, and pelvis of representative volunteers respectively. Example coronal slices are displayed for the brain and head-and-neck (Figs. 5 and 6 respectively) and the middle, axial slice is shown for the pelvic images (Fig. 7). Besides the wrapped (a) and unwrapped (b, c) phase maps, histograms of the unwrapped phase difference between the PRELUDE and SEGUE results (d) and computation times (T_c) are also shown.

In all brain images, the unwrapped phase maps calculated using PRELUDE and SEGUE (see Fig. 5 b and c) looked nearly identical. Fig. 5 d also shows that there were 1000 times more voxels with identical unwrapped phase values than voxels with a 2π phase difference between the PRELUDE and SEGUE results. Moreover, the red arrows indicate a small residual wrap (the phase difference was confirmed to be around 2π) in the PRELUDE result which was successfully resolved in the SEGUE result. Table II shows that the low percentage of differing voxels (<0.4% across all individuals), low mean absolute difference (<0.03 rad), and low maximum difference (<5 · 2π) were consistent across the five healthy volunteers. Moreover, both techniques could unwrap more than 99.9% of the entire brain mask in each case. SEGUE was only slightly faster than PRELUDE at the first echo time, but the difference in T_c drastically increased towards later echoes. At $TE_{max} = 24.6$ ms, SEGUE was about 30 times faster. Note that T_cs were also consistent across volunteers.

In the more challenging head-and-neck and pelvic images (see Figs. 6 and 7) the unwrapped phase images of PRELUDE and SEGUE were still very similar visually. In Fig. 6, the red arrows indicate a residual wrap in the PRELUDE results that was successfully resolved by SEGUE. The histograms of the phase differences (see Figs. 6 and 7 d) indicate at least 100 times more voxels with identical unwrapped phase than voxels with a 2π phase difference for the head-and-neck and pelvic images when the example slices appeared identical on visual comparison. There are more differing voxels (see Figs. 6 and 7 d, green dashed lines) where residual wraps are observed towards the tissue edges or in fatty tissue (see Figs. 6 and 7 b-c, green arrows). Residual wraps

(see Table I) and differences between the unwrapped image and the ground truth were only visible at a very small scale (Fig. 3 d).

Fig. 4 shows the comparison between PRELUDE and SEGUE in the Gaussian phantom with different noise levels. Table I shows that ME was the same for the two techniques for all noise levels. PRELUDE was slightly faster than SEGUE in the phantom with the lowest noise. However, T_c of PRELUDE rapidly increased with increasing noise level (almost 12 hours for the phase map with the highest noise level), whereas SEGUE could unwrap even the phantom with the highest noise level in ≈ 1.5 minutes.
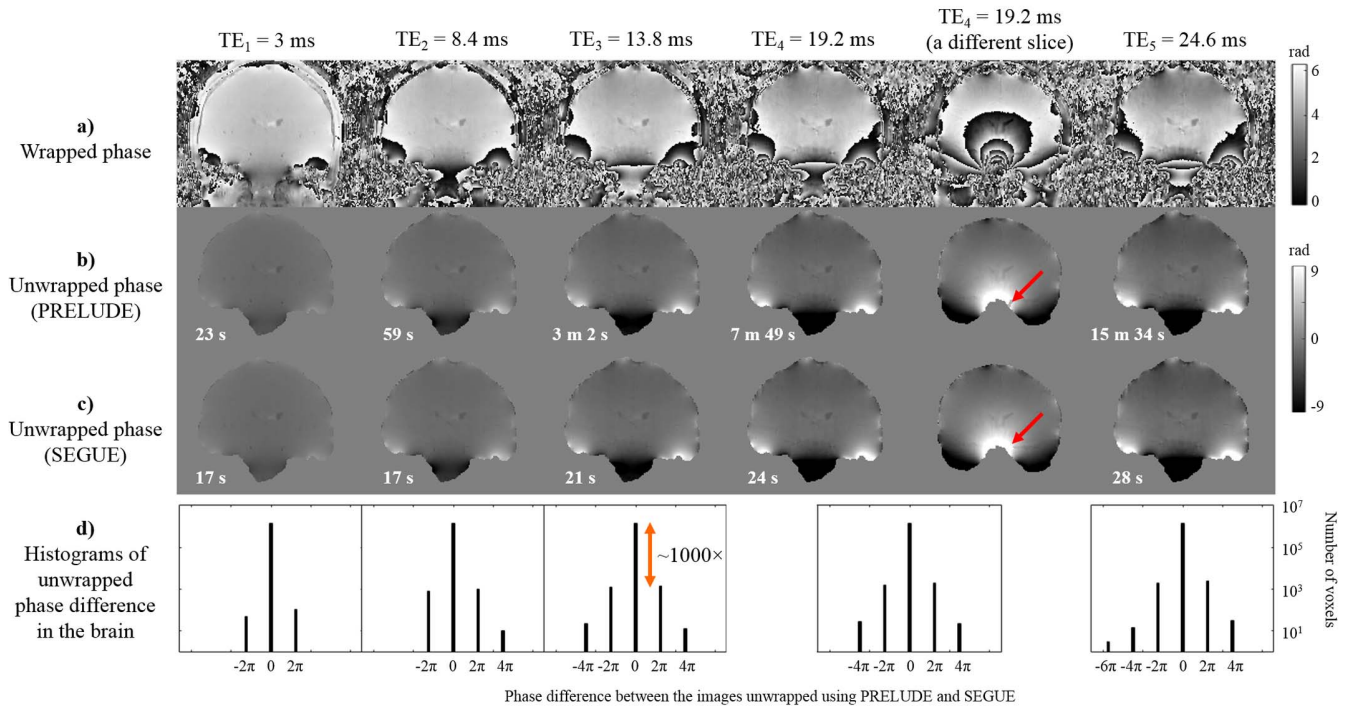
Fig. 5. Unwrapping brain images. Phase maps acquired in the brain of a representative healthy volunteer at five different echo times (a) were unwrapped using either PRELUDE (b) or SEGUE (c). T_C corresponding to each result is shown in the corner of the unwrapped phase maps. A different coronal slice is also shown for TE$_4$ = 19.2 ms. Histograms of the 3D difference images between the PRELUDE and SEGUE results are also displayed (d). The red arrows indicate where SEGUE appears to be more accurate than PRELUDE. There were at least 1000 times more voxels with identical unwrapped phase values in the PRELUDE and SEGUE results than voxels with a 2π phase difference (orange double arrow). Note the logarithmic scale in d.

TABLE II
SUMMARY OF THE RESULTS IN ALL HEALTHY VOLUNTEERS. PERCENTAGES OF THE UNWRAPPED VOXELS (UNVOX) USING EITHER PRELUDE OR SEGUE AND COMPUTATION TIMES (T_c) ARE SHOWN AS WELL AS THE PERCENTAGES OF DIFFERING VOXELS (DIFFVOX), MEAN ABSOLUTE DIFFERENCES (MD), AND THE MAXIMUM DIFFERENCES (MAXDIFF) BETWEEN THE PRELUDE AND SEGUE RESULTS. IN EACH CELL, MEAN ± STANDARD DEVIATION ACROSS HEALTHY VOLUNTEERS ARE SHOWN. THE RED NUMBERS (WITHIN THE RED DASHED RECTANGLES) INDICATE HIGH DIFFVOX AND MD VALUES IN SOME OR ALL OF THE HEALTHY VOLUNTEERS

| | | PRELUDE | | SEGUE | | | | |
	Echo time (ms)	UnVox (%)	T_c	UnVox (%)	T_c	DiffVox (%)	MD (rad)	MaxDiff (rad/2π)
	3	99.98±0.008	22 s ± 4 s	99.97±0.009	16 s ± 1 s	0.03±0.01	0.0019±0.0009	1.4±0.5
	8.4	99.97±0.007	55 s ± 6 s	99.97±0.009	18 s ± 1 s	0.11±0.02	0.007±0.001	1.8±0.5
Brain images (n = 5)	13.8	99.97±0.007	2 m 40 s ± 21 s	99.97±0.005	20 s ± 1 s	0.16±0.03	0.010±0.002	2.0±0.0
	19.2	99.98±0.002	6 m 19 s ± 52 s	99.96±0.004	23 s ± 1 s	0.22±0.03	0.014±0.002	3.0±1.0
	24.6	99.98±0.004	12 m 17 s ± 1 m 52 s	99.95±0.013	26 s ± 2 s	0.31±0.05	0.020±0.003	3.0±0.7
	3	99.8±0.05	16 m 19 s ± 11 m 35 s	99.6±0.20	36 s ± 3 s	0.11±0.20	0.03±0.01	3.0±0.8
Head-and-neck images (n = 4)	8.3	99.8±0.04	3 h 27 m 53 s ± 58 m 2 s	99.4±0.31	2 m 57 s ± 1 m 3 s	7.1±5.6	0.46±0.36	9.5±0.6
	13.6	99.8±0.04	6 h 9 m 21 s ± 57 m 54 s	99.3±0.26	6 m 59 s ± 1 m 35 s	5.6±6.4	0.38±0.41	15.5±2.4
	18.9	99.8±0.04	9 h 47 m 40 s ± 1 h 41 m 40 s	99.3±0.14	17 m 35 s ± 9 m 26 s	6.1±4.2	0.50±0.36	34.3±22.5
	1.17	96.0±5.9	7 m 24 s ± 3 m 52 s	95.8±5.8	18 s ± 6 s	0.74±0.18	0.05±0.01	2.6±0.9
	2.77	96.1±5.9	24 s ± 12 s	95.3±5.6	11 s ± 1 s	0.03±0.03	0.002±0.002	2.0±1.2
Pelvic images (n = 5)	4.37	96.1±5.9	2 m 0 s ± 1 m 12 s	95.9±6.0	13 s ± 3 s	0.74±1.49	0.047±0.094	2.4±0.5
	5.97	96.1±5.9	20 m 56 s ± 8 m 45 s	96.0±5.9	54 s ± 22 s	4.84±1.79	0.35±0.16	8.6±5.4
	7.57	96.1±5.9	9 m 53 s ± 6 m 17 s	95.7±5.8	19 s ± 8 s	1.04±1.44	0.12±0.21	12.6±18.7
	9.17	96.1±5.9	15 m 29 s ± 8 m 15 s	95.1±5.4	29 s ± 16 s	3.57±16.41	0.23±0.45	6.4±3.6

appearing within the subcutaneous fat or fatty fascia were a recurring problem for both PRELUDE and SEGUE. This is partly the reason for the relatively high DiffVox (5-20%) and MD (0.5-1 rad) values at certain echo times in Table II (highlighted in red). Since the head-and-neck and pelvic masks were generated by thresholding the inverse noise map, these
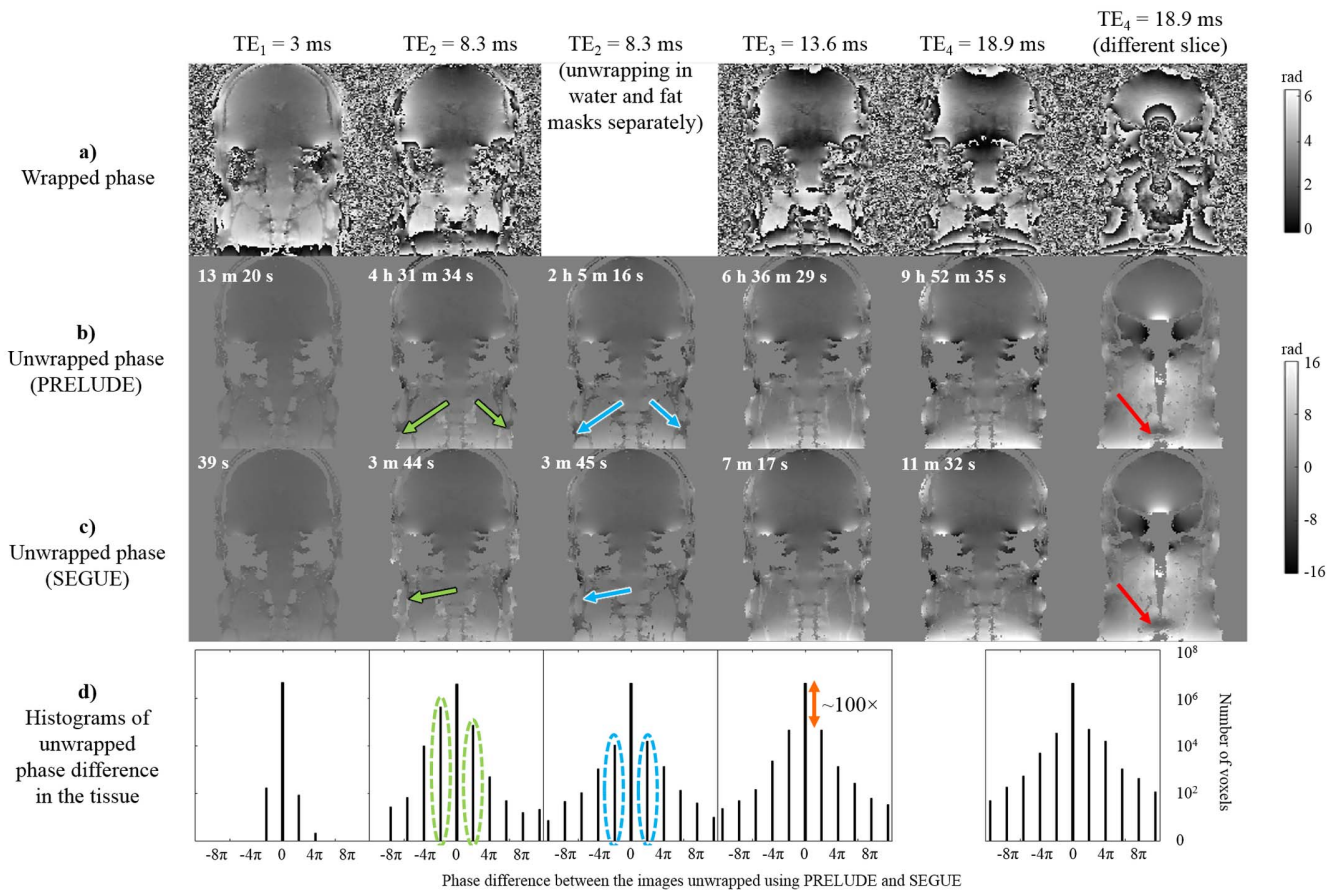
Fig. 6.   Unwrapping head-and-neck images. Phase maps acquired in the head-and-neck of a representative healthy volunteer at four different echo times (a) were unwrapped using either PRELUDE (b) or SEGUE (c). Both techniques were also applied separately in the water and fat masks (example shown in the third column). T_c corresponding to each result is shown in the corner of the unwrapped phase maps. A different coronal slice is also shown for $TE_4 = 18.9$ ms. Histograms of the 3D difference images between the PRELUDE and SEGUE results are also displayed (d). The red arrows indicate where SEGUE seems to be more accurate than PRELUDE. The green arrows with black borders indicate residual wraps in fatty tissue. There were at least 100 times more voxels with identical unwrapped phase values in the PRELUDE and SEGUE results than voxels with a 2π phase difference (orange double arrow) except when residual wraps in fatty tissue were present (green dashed lines). Note the logarithmic scale in d. The blue arrows with white borders indicate the continuous unwrapped phase within the fatty fascia when applying PRELUDE and SEGUE separately in fatty tissue and water-based tissue, while the blue dashed lines highlight the corresponding reduced number of differing voxels.

masks include some small, noisy voxels outside of the tissue that are immediately excluded from the unwrapping by both phase unwrapping techniques as they are not connected to the largest region in the mask. Therefore the UnVox values are a bit lower than for brain images, but both PRELUDE and SEGUE unwrapped more than 99% of the head-and-neck images (across all individuals). For the pelvic images, sometimes the arms of the volunteer appeared next to the pelvis and are also similarly excluded by both PRELUDE and SEGUE, so the UnVox values were even lower (about 90% across all individuals or about 96% on average), but they were similar for the two techniques for all images. In the head-and-neck and pelvic images, SEGUE was about 30 to 70, and 2 to 30 times faster than PRELUDE, respectively. Again, T_cs are reasonably consistent across volunteers.

All head-and-neck and pelvic images were also unwrapped separately within water and fat masks using both PRE-LUDE and SEGUE (see Fig. 6 third column, Fig. 7 last column, and Table III). Note that the head-and-neck images of one volunteer were excluded from the results of Table III

as the fat-water separation failed in this case. The simple strategy of unwrapping within water and fat masks separately successfully removed the residual wraps in fatty tissue (see Figs. 6 and 7 b-c, blue arrows) and resulted in a reduced number of differing voxels (see Figs. 6 and 7 d, blue dashed lines). It also reduced both DiffVox (<4% across all volunteers) and MD (<0.3 rad) for most echo times (see Table III, highlighted in red). DiffVox and MD in the last-echo head-and-neck images were still high (see Table III, highlighted in blue), because there was one volunteer where a large portion of the scalp was not properly unwrapped by SEGUE resulting in DiffVox $\approx$ 15% and MD $\approx$ 1.5. In the remaining volunteers, DiffVox was less than 2.5% and MD was below 0.25 rad, in line with the rest of the results in the head-and-neck. Similarly, the slightly higher DiffVox and MD in the fourth-echo pelvic images (compared to the rest of the echoes) originated from one volunteer where the unwrapping was inconsistent between SEGUE and PRELUDE in a small area of the subcutaneous fat due to imperfect fat-water separation. UnVox values were slightly reduced compared to when
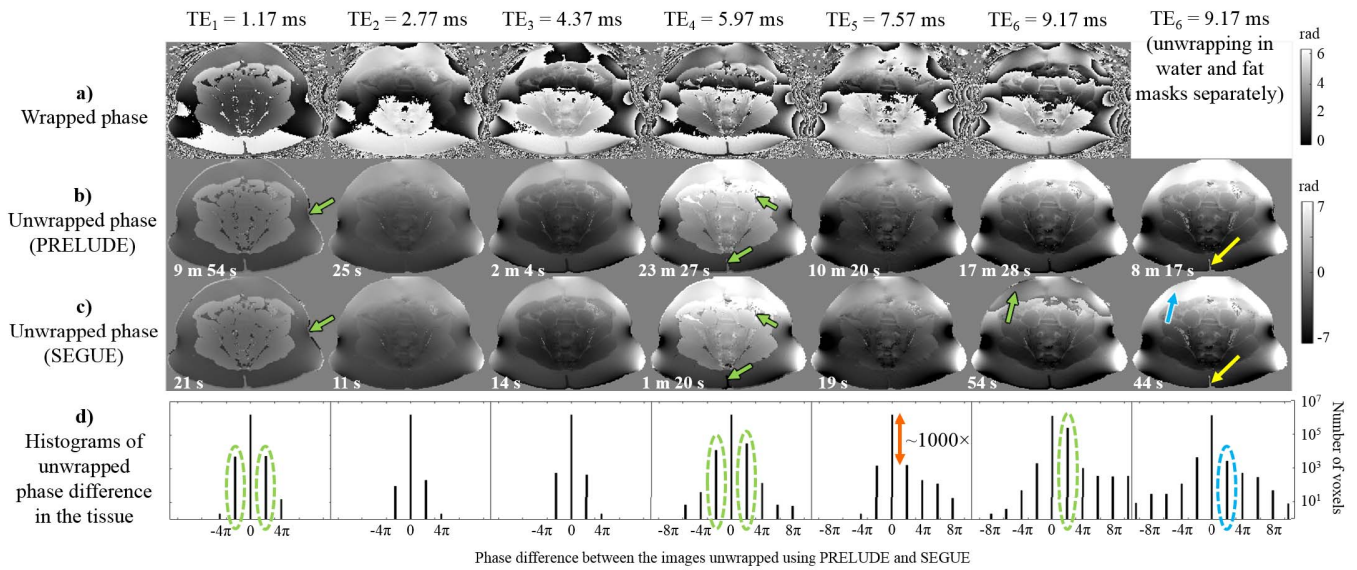
Fig. 7. Unwrapping images of the pelvis. Phase maps acquired in the pelvis of a representative healthy volunteer at six different echo times (a) were unwrapped using either PRELUDE (b) or SEGUE (c). Both techniques were also applied separately in the water and fat masks (example shown in the last column). T_c corresponding to each result is shown in the corner of the unwrapped phase maps. Histograms of the 3D difference images between the PRELUDE and SEGUE results are also displayed (d). The green arrows with black borders indicate residual wraps in fatty tissue. There were at least 1000 times more voxels with identical unwrapped phase values in the PRELUDE and SEGUE results than voxels with a 2π phase difference (orange double arrow) except when the results were visually different in fatty tissue (green dashed lines). Note the logarithmic scale in d. The blue arrow with white border and blue dashed lines indicate how performing the unwrapping separately in the water and fat masks removed the residual wraps in subcutaneous fat. The yellow arrows indicate that the skin was excluded from the unwrapped phase images when PRELUDE or SEGUE were applied separately within the fat and water masks.

TABLE III

SUMMARY OF THE HEAD-AND-NECK AND PELVIC RESULTS WHEN UNWRAPPING SEPARATELY IN THE WATER AND FAT MASKS. PERCENTAGES OF THE UNWRAPPED VOXELS (UNVOX) USING EITHER PRELUDE OR SEGUE AND COMPUTATION TIMES (T_C) ARE SHOWN AS WELL AS THE PERCENTAGES OF DIFFERING VOXELS (DIFFVOX), MEAN ABSOLUTE DIFFERENCES (MD), AND THE MAXIMUM DIFFERENCES (MAXDIFF) BETWEEN THE PRELUDE AND SEGUE RESULTS. IN EACH CELL, MEAN ± STANDARD DEVIATION ACROSS HEALTHY VOLUNTEERS ARE SHOWN. NOTE THAT THE HEAD-AND-NECK IMAGES OF ONE HEALTHY VOLUNTEER WERE EXCLUDED DUE TO A FAILED FAT-WATER SEPARATION. THE RED NUMBERS (WITHIN THE RED DASHED RECTANGLES) INDICATE GREATLY IMPROVED DIFFVOX AND MD VALUES COMPARED TO TABLE II, WHILE THE BLUE NUMBERS (WITHIN THE BLUE DOTTED RECTANGLES) INDICATE VALUES THAT ARE STILL SLIGHTLY HIGH COMPARED TO THE REST OF THE ECHOES

		PRELUDE		SEGUE				
	Echo time (ms)	UnVox (%)	T_c	UnVox (%)	T_c	DiffVox (%)	MD (rad)	MaxDiff (rad/2π)
Head-and-neck images (n = 3)	3	98.2±0.2	10 m 53 s ± 2 m 52 s	97.5±0.6	1 m 14 s ± 7 s	0.12±0.18	0.007±0.01	2.3±0.6
	8.3	98.2±0.2	1 h 40 m 22 s ± 30 m 52 s	96.6±1.1	8 m 1 s ± 6 m 4 s	1.4±1.0	0.14±0.10	24.7±25.4
	13.6	98.2±0.2	3 h 7 m 43 s ± 36 m 44 s	96.3±1.3	17 m 10 s ± 13 m 1 s	1.7±2.1	0.14±0.18	21.0±13.2
	18.9	98.2±0.2	5 h 33 m 26 s ± 58 m 13 s	96.4±1.1	41 m 17 s ± 15 m 47 s	6.5±7.4	0.63±0.73	39.3±27.5
Pelvic images (n = 5)	1.17	92.6±5.1	3 m 44 s ± 2 m 12 s	90.8±4.8	24 s ± 3 s	1.38±0.79	0.12±0.10	4.4±1.1
	2.77	92.6±5.1	27 s ± 10 s	92.2±5.1	20 s ± 2 s	0.03±0.03	0.002±0.002	2.8±0.4
	4.37	92.6±5.1	1 m 27 s ± 22 s	92.2±5.1	26 s ± 6 s	0.08±0.08	0.006±0.006	3.8±0.4
	5.97	92.5±5.1	8 m 44 s ± 3 m 23 s	91.6±4.9	43 s ± 16 s	1.69±0.76	0.11±0.05	7.0±1.6
	7.57	92.5±5.1	4 m 51 s ± 2 m 10 s	92.0±5.0	36 s ± 14 s	0.66±0.77	0.06±0.08	17.8±23.7
	9.17	92.5±5.1	7 m 44 s ± 2 m 49 s	92.0±5.2	52 s ± 28 s	0.54±0.46	0.04±0.03	9.8±4.1

PRELUDE and SEGUE were applied in the entire tissue mask at once, because both techniques perform the unwrapping only in the largest connected region of the tissue mask. Therefore, for example the water-based skin was not unwrapped in many pelvic images (see Fig. 7, yellow arrows) as it was separated from the rest of the water-based tissue by the subcutaneous fat. However, the UnVox percentages were still similar for PRELUDE and SEGUE in all images. PRELUDE was usually about twice as fast when unwrapping in the fat and water masks separately, while SEGUE was slightly slower in each case. However, SEGUE was still about 10 times faster than PRELUDE in most cases (except in the second- and third-echo pelvic images, where it was only 1.3 and 3 times faster on average). Finally, note that MaxDiff was much higher

in these challenging anatomical regions (head-and-neck and pelvis) than in brain images both with and without unwrapping separately within fat and water masks. In summary, applying PRELUDE or SEGUE separately within fat and water masks improves the unwrapped phase images with no great increase in computation time.

V. DISCUSSION

We have developed SEGUE, a new, fast phase unwrapping algorithm based on similar principles to the state-of-the art method, PRELUDE. The unwrapping is accelerated in SEGUE by always using 3D partitioning and by simultaneous unwrapping and merging of several regions. We compared SEGUE with PRELUDE in numerical phantoms and using in-vivo images of the brain, head-and-neck, and pelvis. SEGUE provided almost identical results to PRELUDE in each case, but was up to 70 times faster depending on the echo time and anatomical region. We have also shown that applying either technique within water and fat masks separately successfully removed residual wraps in fatty tissue and resulted in more similar unwrapped phase maps between PRELUDE and SEGUE.

For images acquired at short echo times, PRELUDE [20], [21] and SEGUE often had similar computation times (T_c). However, with increasing echo time, the phase images contained more wraps which exponentially increased the number of initial, 2D regions and, consequently, T_c of PRELUDE. Since the number of the initial 3D regions increased much more slowly, SEGUE could unwrap severely wrapped phase images at later echoes very quickly compared to PRELUDE. Both the histograms of the difference images and the measured DiffVox values confirmed that most voxels had identical unwrapped phase values in the PRELUDE and SEGUE results. In case of the brain images, this was the overwhelming majority of the voxels (differing voxels <0.4%) in every image.

Unwrapping the head-and-neck and pelvic images using either PRELUDE or SEGUE proved to be more challenging. One of the issues is the presence of fatty tissue (fascia and/or subcutaneous fat) that led to residual wraps in the unwrapped phase images. In most anatomical regions, the majority of voxels are water-based and the fatty tissue is usually completely surrounded by these water-filled voxels (e.g. fatty fascia between the muscle sheets). Therefore, the regions partitioned within the fatty tissue often have a larger border with the neighbouring water-based regions than with other fatty regions. Consequently, at the unwrapping and merging step of the algorithms, the phase within fatty regions is compared to the phase of the water-based regions rather than the phase in other fatty tissue. However, the phase in fatty regions has an additional, chemical-shift-induced component. If the chemical-shift-induced phase difference between fatty and water-based regions is close to π, the calculated phase offset (either 0 or 2π) is expected to be arbitrary and largely dependent on the local noise level. This is a recurring problem for both PRELUDE and SEGUE in anatomical regions containing fatty tissue. Here, we have shown
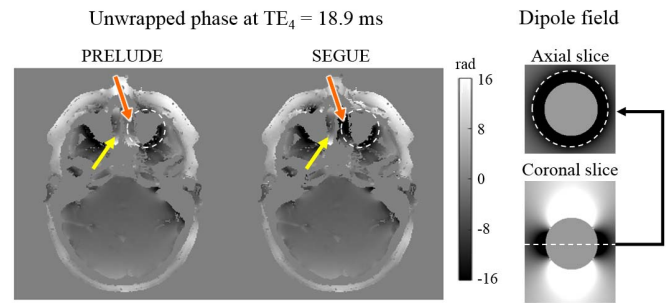

Fig. 8. Unwrapped phase around the nasal septum in the last-echo head-and-neck image of the representative volunteer. The dashed lines indicate the expected shape of the dipolar phase variations induced by the susceptibility difference between tissue and the air in the nasal sinuses. The orange arrows with white borders indicate the tissue on the right side of the nasal septum that only SEGUE could unwrap successfully, while the yellow arrows indicate the left side where both techniques failed.

that applying these techniques in the fat and water masks separately can resolve this issue. A limitation of this approach is that fat-water separation is needed to generate separate fat and water masks. In addition, for most fat-water separation techniques, multi-echo data are needed and the quality of the separation might depend on the echo timing [32]. Furthermore, current fat-water separation strategies do not necessarily work in every image (e.g. the three-point Dixon method failed in one of the head-and-neck images even though it was acquired using the same sequence and parameters as the others). Moreover, the quality of the fat-water separation affects the quality of the phase unwrapping as seen in one of the pelvic images with imperfect fat-water separation.

Applying PRELUDE and SEGUE within fat and water masks separately substantially increased the number of identical voxels in both the head-and-neck and the pelvis. The percentage of differing voxels (DiffVox) is still slightly higher in general in the head-and-neck images than in the brain or pelvic images. This is due to some smaller regions in the head-and-neck (such as the tissue around the nasal septum, Fig. 8, arrows) being connected to the bulk of the tissue by only a few voxels within the tissue mask making it hard to estimate their corresponding phase offset. Therefore, sometimes these regions had different phase offsets in the PRELUDE and SEGUE results (Fig. 8, orange arrows). Based on the approximate shape of the phase variations expected to be induced by the susceptibility difference between tissue and air in the sinuses (Fig. 8, dipole field and dashed lines), it seems that only SEGUE could unwrap the tissue on the right side of the nasal septum (Fig. 8, orange arrows), while both PRELUDE and SEGUE failed on the left (Fig. 8, yellow arrows). The same problem occurred in one of the last-echo head-and-neck images when a large part of the scalp was unwrapped incorrectly as it was connected to the bulk of the tissue by only a few voxels in the water mask. Identifying a more robust fat-water separation technique and creating more accurate tissue masks tailored for specific clinical applications are beyond the scope of this study but these steps would definitely help mitigate these remaining issues with phase unwrapping in challenging areas of the body. Also, note that

though the three-point Dixon method failed in one out of the four head-and-neck images, fat-water separation errors were present only in one pelvic image out of five and even these were restricted to a small area at the outer edges of the subcutaneous fat. Moreover, all the regions where PRELUDE and SEGUE provided different results, due to them being connected to the rest of the tissue by only a few voxels, were in areas that are not generally the focus of MRI studies (e.g. nasal septum, eyeballs, or scalp).

The large MaxDiff values in a few voxels towards the edges of the tissue (see Table II, especially the head-and-neck results) are induced by noisy voxels. SEGUE estimates the phase offset by linear extrapolation using phase values in two neighbouring voxels. If both of these voxels are noisy, the extrapolated, estimated phase is likely to be very inaccurate. PRELUDE uses a single nearest-neighbor extrapolation, which is less likely to induce extremely high unwrapped phase values. However, near large phase gradients, the unwrapped phase values of neighbouring voxels are not close to each other so nearest-neighbour extrapolation is expected to fail, whereas linear extrapolation should provide more accurate results. The measured MaxDiff values are larger for head-and-neck images, because this anatomical region contains larger susceptibility gradients (e.g. at the tissue/air interfaces around the sinuses) inducing highly-variable phase. More careful masking of these noisy voxels towards the mask edges could eliminate these effects.

Note that due to the 3D partitioning, SEGUE is expected to be less robust than PRELUDE to open-ended fringe lines (OFs), i.e. wraps that do not reach the edge of the tissue [34], but suddenly stop within the tissue (Fig. 9 a, yellow arrow). At the partitioning step, the gray voxels in Fig. 9 a (highlighted by the dashed line) can form a single region when there should be a 2π difference between region A and region B due to the wrap indicated by the arrow. This situation can occur for several different reasons. Some MRI systems perform a coil combination technique after multi-channel acquisitions that results in incorrect phase values [19] and large OFs in the tissue (Fig. 9 a). Highly-variable phase due to large susceptibility gradients and/or motion can also induce OFs (Fig. 9 b). Small open-ended fringe lines can form when a voxel along a wrap contains spins with phases close to both $+\pi$ and $-\pi$. Since the measured phase is the phase of the complex sum of spins with these individual phase values, the voxel appears gray (≈ 0 rad) instead of black ($+\pi$) or white ($-\pi$) forming a partial volume open-ended fringe line (Fig. 9 c). 2D partitioning can mitigate the effects of all kinds of open-ended fringe lines, because the 2D regions tend to be very small. Incorrect unwrapping of one of the 2D regions does not necessarily propagate into other parts of the image. In contrast, 3D partitions can be large, connecting regions that are very far from each other, leading to long-ranging effects. However, using 2D partitioning greatly increases the number of initial regions everywhere, not just around open-ended fringe lines. Therefore this approach is very inefficient in dealing with this problem. Note that the approach SEGUE uses for partitioning (removing the small bridges between larger regions before identifying the initial, connected regions) seems
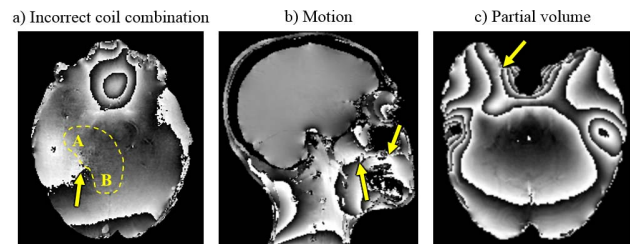

Fig. 9. Open-ended fringe lines can occur e.g. due to incorrect coil combination in multi-channel imaging (a), highly-variable phase due to large susceptibility gradients and/or motion (b), or partial volume effects (c).

to be able to deal with most types of OFs. OFs due to incorrect coil-combination are expected to cause more problems for SEGUE than for PRELUDE, but these can be avoided by combining the phase images from multiple coils correctly at the earlier image reconstruction step [19].

Finally, note that while testing SEGUE in phase images acquired using other modalities is beyond the scope of this study, the SEGUE algorithm is not specific to MR images and could be applied more broadly in future.

VI. Conclusions

We have developed SEGUE, a spatial phase unwrapping technique that was found to be 1.5 to 70 times faster than the gold-standard, PRELUDE, and produced similarly accurate results. SEGUE could provide an alternative to PRELUDE, especially for highly wrapped, high-resolution images. We have also shown that performing phase unwrapping separately within the fat and water masks in challenging anatomical regions led to more accurate results in both PRELUDE and SEGUE. Separate fat and water unwrapping is an option available within SEGUE. SEGUE (downloadable from https://xip.uclb.com/i/software/SEGUE.html) promises to accelerate and improve phase unwrapping for a broad range of MR phase imaging applications from Quantitative Susceptibility Mapping to distortion correction in functional and diffusion MRI.

References

[1] C. Liu, W. Li, K. A. Tong, K. W. Yeom, and S. Kuzminski, "Susceptibility-weighted imaging and quantitative susceptibility mapping in the brain," *J. Magn. Reson. Imag.*, vol. 42, no. 1, pp. 23–41, 2015.

[2] Y. Wang *et al.*, "Artery and vein separation using susceptibility-dependent phase in contrast-enhanced MRA," *J. Magn. Reson. Imag.*, vol. 12, no. 5, pp. 661–670, 2000.

[3] E. M. Haacke, Y. Xu, Y.-C. N. Cheng, and J. R. Reichenbach, "Susceptibility weighted imaging (SWI)," *Magn. Reson. Med.*, vol. 52, no. 3, pp. 612–618, 2004.

[4] K. Shmueli, J. A. de Zwart, P. van Gelderen, T.-Q. Li, S. J. Dodd, and J. H. Duyn, "Magnetic susceptibility mapping of brain tissue *in vivo* using MRI phase data," *Magn. Reson. Med.*, vol. 62, no. 6, pp. 1510–1522, 2009.

[5] Y. Wang and T. Liu, "Quantitative susceptibility mapping (QSM): Decoding MRI data for a tissue magnetic biomarker," *Magn. Reson. Med.*, vol. 73, no. 1, pp. 82–101, 2015.

[6] J. Reichenbach, F. Schweser, B. Serres, and A. Deistung, "Quantitative susceptibility mapping: Concepts and applications," *Clin. Neuroradiol.*, vol. 25, no. 2, pp. 225–230, 2015.

[7] E. M. Haacke, S. Liu, S. Buch, W. Zheng, D. Wu, and Y. Ye, "Quantitative susceptibility mapping: Current status and future directions," *Magn. Reson. Imag.*, vol. 33, no. 1, pp. 1–25, 2015.

[8] S. Eskreis-Winkler et al., "The clinical utility of QSM: Disease diagnosis, medical management, and surgical planning," *NMR Biomed.*, vol. 30, no. 4, p. e3668, 2017.

[9] J. Ahveninen et al., "Intracortical depth analyses of frequency-sensitive regions of human auditory cortex using 7T fMRI," *NeuroImage*, vol. 143, pp. 116–127, 2016.

[10] J. Ashburner, "Preparing fMRI data for statistical analysis," in *fMRI Techniques and Protocols*. New York, NY, USA: Humana Press, 2016, pp. 155–181.

[11] P. Branco, D. Seixas, and S. L. Castro, "Temporal reliability of ultrahigh field resting-state MRI for single-subject sensorimotor and language mapping," *NeuroImage*, vol. 168, pp. 499–508, Mar. 2016.

[12] P. L. Cardoso et al., "The clinical relevance of distortion correction in presurgical fMRI at 7 T," *NeuroImage*, vol. 168, pp. 490–498, Mar. 2016.

[13] J. C. Brooks, W.-E. Davies, and A. E. Pickering, "Resolving the brainstem contributions to attentional analgesia," *J. Neurosci.*, vol. 37, no. 9, pp. 2279–2291, 2017.

[14] M. S. Graham, I. Drobnjak, M. Jenkinson, and H. Zhang, "Quantitative assessment of the susceptibility artefact and its interaction with motion in diffusion MRI," *PLoS ONE*, vol. 12, no. 10, p. e0185647, 2017.

[15] K. Shen et al., "A spatio-temporal atlas of neonatal diffusion MRI based on kernel ridge regression," in *Proc. IEEE 14th Int. Symp. Biomed. Imag. (ISBI)*, Apr. 2017, pp. 126–129.

[16] M. M. Herting, R. Kim, K. A. Uban, E. Kan, A. Binley, and E. R. Sowell, "Longitudinal changes in pubertal maturation and white matter microstructure," *Psychoneuroendocrinology*, vol. 81, pp. 70–79, Jul. 2017.

[17] V. Rajagopalan and E. P. Pioro, "Differential involvement of corticospinal tract (CST) fibers in UMN-predominant ALS patients with or without cst hyperintensity: A diffusion tensor tractography study," *NeuroImage, Clin.*, vol. 14, pp. 574–579, Feb. 2017.

[18] R. Kemppainen, S. Suilamo, T. Tuokkola, P. Lindholm, M. H. Deppe, and J. Keyriläinen, "Magnetic resonance-only simulation and dose calculation in external beam radiation therapy: A feasibility study for pelvic cancers," *Acta Oncologica*, vol. 56, no. 6, pp. 792–798, 2017.

[19] S. D. Robinson, K. Bredies, D. Khabipova, B. Dymerska, J. P. Marques, and F. Schweser, "An illustrated comparison of processing methods for MR phase imaging and QSM: Combining array coil signals and phase unwrapping," *NMR Biomed.*, vol. 30, no. 4, p. e3601, 2016.

[20] M. Jenkinson, "Fast, automated, N-dimensional phase-unwrapping algorithm," *Magn. Reson. Med.*, vol. 49, no. 1, pp. 193–197, 2003.

[21] M. Jenkinson, C. F. Beckmann, T. E. Behrens, M. W. Woolrich, and S. M. Smith, "FSL," *NeuroImage*, vol. 62, no. 2, pp. 782–790, 2012.

[22] J. Dong et al., "Simultaneous phase unwrapping and removal of chemical shift (SPURS) using graph cuts: Application in quantitative susceptibility mapping," *IEEE Trans. Med. Imag.*, vol. 34, no. 2, pp. 531–540, Feb. 2015.

[23] A. V. Dimov et al., "Joint estimation of chemical shift and quantitative susceptibility mapping (chemical QSM)," *Magn. Reson. Med.*, vol. 73, no. 6, pp. 2100–2110, 2015.

[24] S. D. Sharma et al., "MRI-based quantitative susceptibility mapping (QSM) and R2* mapping of liver iron overload: Comparison with SQUID-based biomagnetic liver susceptometry," *Magn. Reson. Med.*, vol. 78, no. 1, pp. 264–270, 2017.

[25] H. Wei et al., "Investigating magnetic susceptibility of human knee joint at 7 Tesla," *Magn. Reson. Med.*, vol. 78, no. 5, pp. 1933–1943, 2017.

[26] A. Karsa, S. Punwani, and K. Shmueli, "Fat correction of MRI phase images for accurate susceptibility mapping in the head-and-neck," in *Proc. ISMRM 26th Annu. Meeting*, Paris, France, 2018, p. 4988.

[27] A. Karsa and K. Shmueli, "SEGUE: A speedy rEgion-growing algorithm for unwrapping estimated phase," in *Proc. ISMRM 26th Annu. Meeting*, Paris, France, 2018, p. 666.

[28] S. Robinson, H. Schödl, and S. Trattnig, "A method for unwrapping highly wrapped multi-echo phase images at very high field: UMPIRE," *Magn. Reson. Med.*, vol. 72, no. 1, pp. 80–92, 2014.

[29] T. J. Bray, A. Bainbridge, S. Punwani, Y. Ioannou, and M. A. Hall-Craggs, "Simultaneous quantification of bone edema/adiposity and structure in inflamed bone using chemical shift-encoded MRI in spondyloarthritis," *Magn. Reson. Med.*, vol. 79, no. 2, pp. 1031–1042, 2018.

[30] S. M. Smith, "Fast robust automated brain extraction," *Hum. Brain Mapping*, vol. 17, no. 3, pp. 143–155, 2002.

[31] B. Kressler, L. de Rochefort, T. Liu, P. Spincemaille, Q. Jiang, and Y. Wang, "Nonlinear regularization for per voxel estimation of magnetic susceptibility distributions from MRI field maps," *IEEE Trans. Med. Imag.*, vol. 29, no. 2, pp. 273–281, Feb. 2010.

[32] J. Berglund, L. Johansson, H. Ahlström, and J. Kullberg, "Three-point Dixon method enables whole-body water and fat imaging of obese subjects," *Magn. Reson. Med.*, vol. 63, no. 6, pp. 1659–1668, 2010.

[33] H. H. Hu et al., "ISMRM workshop on fat–water separation: Insights, applications and progress in MRI," *Magn. Reson. Med.*, vol. 68, no. 2, pp. 378–388, 2012.

[34] S. Chavez, Q.-S. Xiang, and L. An, "Understanding phase maps in MRI: A new cutline phase unwrapping method," *IEEE Trans. Med. Imag.*, vol. 21, no. 8, pp. 966–977, Aug. 2002.